CHEMISTRY OF MATERIALS

pubs.acs.org/cm

Article

Chemical Design of Efficient Photoelectrodes by Heterogeneous Nucleation of Carbon Dots in Mesoporous Ordered Titania Films

Published as part of the Chemistry of Materials virtual special issue "In Honor of Prof. Clement Sanchez".

Facundo C. Herrera, Veronica Sireus, Pietro Rassu, Luigi Stagi, Marco Reale, Alice Sciortino, Fabrizio Messina, Galo J. A. A. Soler-Illia, Luca Malfatti,* and Plinio Innocenzi*

Cite This: *Chem. Mater.* 2023, 35, 8009–8019

Read Online

ACCESS | Metrics & More | Article Recommendations | Supporting Information

ABSTRACT: The design of efficient and highly durable photoelectrodes requires innovative solutions that can be integrated into thin-film-based technologies. Mesoporous ordered titania, which is characterized by an organized porosity in the 2−10 nm range, represents an ideal matrix for such a purpose. One of the main challenges is the homogeneous and controlled incorporation of photoactive nanoparticles inside the matrix. Titania-carbon dots (C-dots) heterostructures represent promising candidates, but a method to homogeneously introduce C-dots in mesoporous films is still missing. In the present work, C-dots have been nucleated and grown within a mesoporous titania film through in situ solvothermal synthesis. The process promotes the crystallization of titania anatase at low temperatures and at the same time allows the formation of carbon dots without disruption of the porous ordered structure. The process allows building a high-performance nanocomposite as an electrode for oxygen evolution reactions. Photocurrent production under different illumination conditions was measured by linear sweep voltammetry and chronoamperometry. When exposed to a solar simulator, the nanocomposite electrodes yield an increase in photocurrent compared to bare TiO_2 matrices. The better performance has been associated with the presence of C-dots acting as active light-harvesting sites and as charge donors to the photoactive centers of the titania film.

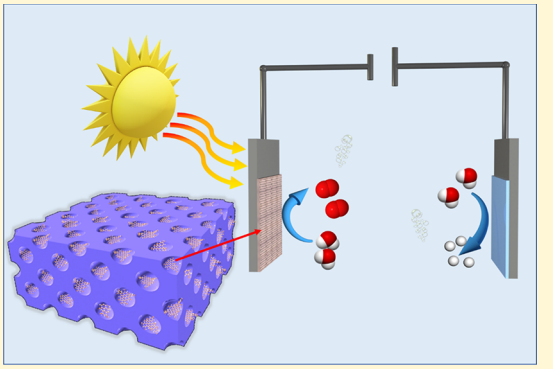

1. INTRODUCTION

Mesoporous thin films obtained via evaporation-induced self-assembly are characterized by an array of monodispersed pores with a defined symmetry and space group.[1,2] The organized, monodispersed mesoporosity (2−50 nm) has the advantage of ensuring reproducible control of surface area per gram of matter. Another advantage is the modulation of diffusivity because the pore shape, dimension, and orientation can be precisely predefined through the design of the topological distribution of mesoporosity.[3−5] The ordered mesoporosity also represents an ideal platform for hosting nanoparticles, enabling the preparation of nanocomposites where the dispersed phase follows the mesopore structural organization.[6,7] Several heterostructures between oxide, metallic, and semiconductor nanoparticles and mesoporous matrices have been reported in the literature.[8−12] Ceria nanoparticles that have been nucleated in a preformed titania matrix through deep X-ray lithography are a significant example of this strategy.[13] Mesoporous ordered silica films having either spherical or cylindrical pores, for instance, have been used to grow FeCo nanocrystals, with the nanopore diameter that gives the upper limit for the nanoparticle size.[14] Moreover, mesoporous ordered titania films have also been employed to form silver nanoparticles through impregnation with silver nitrate and irradiation with UV light. The resulting nanoparticles exhibit a well-defined plasmonic band indicating a monodisperse size of the silver nanostructures with a major diameter of around 10 nm.[15] Another class of nanoparticles that has been successfully incorporated into mesoporous materials are carbon dots (C-dots).[16,17] The family of C-dots consists of a wide variety of carbon-based 0D nanostructures that generally exhibit strong fluorescence and size smaller than 10−20 nm.[18,19] The origin of the emission can be of different nature since the structure of C-dots shows great variability that depends on the synthesis conditions.[20−22] C-dots can have quantum properties when their structure is purely graphitic, and in this case, they are referred to as graphene quantum dots

Received: May 18, 2023
Revised: August 23, 2023
Published: September 7, 2023

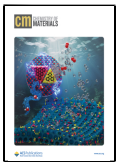

(GQDs).[23−25] The photophysical properties of these nanoparticles are controlled by quantum confinement effects. This makes the GQDs the C-dots with the largest potential in terms of customization and functional design. Carbon quantum dots (CQDs) are intermediate cases. They have a graphitic crystalline core structure, mainly composed of sp^2 hybridized atoms, while the surface is mostly composed of carbon in sp^3 and oxygen and nitrogen-based functional groups. The quantum confinement within the graphitic core controls the luminescence that can be tuned by modulating the size and surface functionalization. However, C-dots can have an amorphous structure and this is the case with carbon nanodots (CNDs). In CNDs, carbon is mostly found in the sp^3 state, although sp^2 domains can still be formed. Photoluminescence is not controlled by quantum confinement but by the presence of molecular fluorophores formed during pyrolysis of the precursors.[26] Finally, one can also obtain carbonized polymer dots (CPDs) that form when amorphous carbon and polymers cross-link to form a hybrid structure.[27]

Although the fabrication of nanocomposites formed from C-dots and mesoporous films is still unexplored, it opens the way for important functional applications in thin-film devices. Several examples of C-dots embedded in polymer thin films have been reported.[28−30] However, the organic polymeric matrices do not have functional properties such as titania oxide, and their possible applications are rather limited. Using mesoporous films to fabricate nanocomposites with C-dots offers the advantage of allowing in situ particle growth. The C-dots, therefore, will have a controlled shape and size while forming functional heterostructures whose chemical−physical interactions at the dot−matrix interface govern the properties. This synthesis, however, while appearing simple as a strategy, is not straightforward and poses several challenges to be solved. One of these is to avoid the formation of agglomerates or a surface layer that would obstruct mesopore access. To solve these issues, we developed a two-stage synthesis; in the first step, the mesoporous titania films are fabricated, and in the second one, they are put in a reactor in solvothermal conditions in situ growth of C-dots. The mesopores become nucleation sites of C-dots leading to the formation of a heterostructure. The material has been tested as a proof-of-concept electrode for oxygen evolution reaction (OER) in water splitting. This device aims to improve the overall efficiency of hydrogen generation from water by engineering the photoanodic material, which is the usual "bottleneck" of the reaction.[31] In the nanocomposite electrode, the carbon-based nanoparticles act as photosensitizers, light-harvesting centers, and/or charge scavengers to enhance the photoactivity of titania.[32] In this regard, the engineering of heterojunctions at the nanoscale has already proven to be effective in boosting the spatial separation and lifetime of photogenerated charges. The electronic coupling of well-defined π states of graphene quantum dots with a catalytic compound, such as a mesoporous ordered titania matrix, is particularly advantageous as it can lead to the formation of heterojunctions with strong solar sensitivity, long photogenerated charges lifetime and, therefore, efficient water splitting.[33,34]

2. EXPERIMENTAL METHODS

2.1. Materials. *2.1.1. Chemicals.* $TiCl_4$ (Sigma-Aldrich, >99%), tetraethylorthosilicate (TEOS) (Sigma-Aldrich, 98%), methyltriethoxysilane (MTES) (Sigma-Aldrich, 99%), ethanol (Sigma-Aldrich, >99.8%), water (milli-Q), phloroglucinol (PG) (Sigma-Aldrich, >99%), and triblock copolymer Pluronic F127 (PEO106-PPO70-PEO106, Aldrich) were used as received without further purification. Silicon wafers (Si-Mat) (100) cut, p-type boron doped, 350 μm thick, silica glasses (Heraeus), SUPRASIL 2 grade B, 1 mm thick, and SnO_2:F coated (FTO) glass slides, 1 mm thick were used as substrates for film deposition.

2.1.2. Synthesis of Mesoporous Thin Films. An adaptation of previously developed procedures was used to prepare the mesoporous thin films.[35,36] For titania mesoporous thin films, briefly, 1.6 cm^3 (0.014 mol) of $TiCl_4$ were dissolved under stirring in 8.4 cm^3 (0.14 mol) of ethanol to give a yellow and transparent stock solution with a molar ratio of $TiCl_4$:EtOH = 1:10. Meanwhile 0.138 g (1.03×10^{-5} mol) of Pluronic F127 were dissolved in 7.35 cm^3 of ethanol (0.126 mol). Then, 1.47 cm^3 of the stock solution $TiCl_4$:EtOH were added, and the transparent mixture was stirred for 5 min until homogenization. Finally, 0.588 cm^3 (0.03 mol) of milli-Q water were poured and the resulting sol was stirred in a closed vial for 2 h at room temperature before utilization. The molar ratios in the final precursor solution are $TiCl_4$:EtOH:H_2O:F127 = 1:69.7:15.5:4×10^{-3}.

For silica mesoporous thin films, 8.93 cm^3 (0.04 mol) of TEOS and 3.19 cm^3 (0.022 mol) of MTES were poured in 9.74 cm^3 (0.17 mol) of ethanol and stirred for 5 min to homogenize the mixture. Then, 0.84 cm^3 (0.062 mol) of water and 0.36 cm^3 of HCl were added to the solution that was stirred for another hour. Meanwhile, a template solution was prepared by mixing 1.3 g of Pluronic F127, 1.5 cm^3 of ethanol, and 1.5 cm^3 of HCl 5×10^{-3} M. Finally, 7.7 cm^3 of the silane solution were added to the template solution that was aged for 4 days. The molar ratios in the final precursor solution are TEOS:MTES:EtOH:H_2O:HCl:F127 = 1:0.56:24:48:14.7:0.11:7.6×10^{-3}.

The substrates were initially cleaned with detergent, water, acetone, and ethanol; then, they were stored in ethanol until further use. Thin films were deposited by dip-coating on the substrates (i.e., silicon wafers and silica slides) with a withdrawal speed of 10 cm min^{-1}. Each substrate was immersed in the precursor solution for 30 s before being withdrawn. The relative humidity (RH) inside the deposition chamber was accurately kept in the range of 21−23 or 40−42% for the titania and silica-based films, respectively; the temperature was kept at 25 °C. After dip-coating, each sample was dried in an oven in the air at 60 °C for 15 min and then annealed in air at 350 °C for 3 h.

2.1.3. Synthesis and Nucleation of Phloroglucinol C-Dots in Mesoporous Thin Films. According to a previously reported procedure, 500 mg of PG were dissolved in 10 cm^3 of ethanol by sonicating the mixture for 10 min.[38] The pale yellow solution was poured into a poly(tetrafluoroethylene) (Teflon)-lined autoclave (25 cm^3) and one mesoporous thin film was immersed inside it. The solvothermal process was repeated several times using the same autoclave to grow the C-dots on both silica and titania mesoporous samples. The mesoporous films that underwent the solvothermal treatment were previously deposited on an FTO and silicon substrates and then treated at 350 ° C for 3 h in air. Then, the autoclave was sealed and heated at 200 °C for 3 h. After the solvothermal reaction, the reactor was cooled to 25 °C. The mesoporous thin films functionalized with C-dots were removed from the solution, rinsed abundantly with ethanol, and dried at room temperature; no further processing was carried out before use. The solution with the C-dots was stored in glass vials for further characterization. The reference samples for XANES analysis were prepared by using a mesoporous titania film deposited on a silicon substrate and treated at 350 °C. The films were solvothermally treated in pure ethanol at 200 °C for 3 h. Other reference samples for transient absorption (TA) analysis were prepared by soaking thermally treated mesoporous titania films (350 °C for 3 h in air) deposited on silica slides. The films were immersed into an ethanol solution of C-dots obtained by following the previously reported solvothermal synthesis. After soaking, the films were left drying in air.

2.2. Characterization Techniques. UV−vis spectroscopy in the transmission mode of the bare titania films and functionalized with C-dots was measured in the range of 200−700 nm with a bandwidth of 1.5 nm using a UV−Vis Nicolet Evolution 300 spectrophotometer.

https://doi.org/10.1021/acs.chemmater.3c01164
Chem. Mater. 2023, 35, 8009−8019

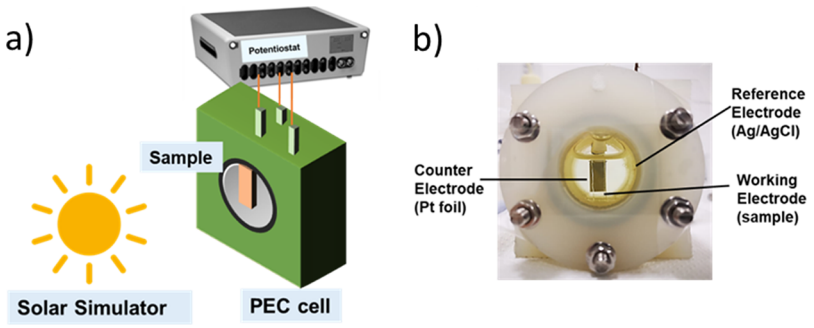

Figure 1. (a) Experimental setup scheme for photoelectrochemical measurements. (b) Custom-made photoelectrochemical cell with a standard 3-electrode system [working electrode (WE): nanocomposite film or bare mesoporous titania, reference electrode (RE): Ag/AgCl (KCl 3 M), counter electrode (CE): Pt foil].

Fourier transform infrared (FTIR) analysis was performed on the films deposited on silicon substrates using a Bruker infrared Vertex 70v. Absorption spectra were acquired in the 4000−400 cm^{-1} range by averaging 128 scans with 4 cm^{-1} resolution. Background evaluation was done by measuring the infrared absorption of a clean silicon wafer substrate; the baseline was fitted with a concave rubber band correction with OPUS 7.0 software.

TEM observations have been performed by an FEI TECNAI 200 operating at 200 kV. Samples were prepared by dispersing a few milligrams in absolute ethanol using an ultrasonic bath. Finally, one or two drops of the as-obtained suspension were dispersed on a holey carbon-supported grid.

A Wollam-α spectroscopic ellipsometer with fixed angle geometry was used to evaluate the thickness and optical constants n and k of thin films deposited on silicon substrates. Sample parameters were estimated using a reference titania sample. The coefficients of the Cauchy model were fitted from the measure of a sol−gel dense titania film treated at 350 °C. These parameters were used to estimate the thickness and porosity of the mesoporous titania films through an effective medium approximation (EMA) model including voids and titania matrix. Finally, the nanocomposite film was fitted using the porosity obtained from the previous measurements as a starting value and considering the C-dots titania matrix as an absorbing material. For each fit, the mean square error (MSE) was kept under 15.

X-ray absorption (XAS) spectra were measured at the XAS beamline of the Elettra Synchrotron (Trieste, Italy). XANES spectra at the Ti K-edge (4966 eV) were recorded in air at 25 °C in fluorescence mode. The intensity I_0 of the incident photon beam was determined by an ionization chamber mounted before the sample, and the fluorescence intensity, I_f, from the sample was measured by averaging the signal from 16 solid-state detectors. The spectra of the samples were expressed as I_f/I_0. All spectra were calibrated using a Ti metallic foil obtained by measuring the intensities I_0 and I_1 from the ionization chambers placed before and after the reference sample. The first point of inflection was used to determine the energy edge absorption position. Ti spectra were recorded using a Si(111) single crystal, which was used as a monochromator.

X-ray reflectometry (XRR) measurements were performed with Bruker D8 Eco equipment using an incident beam of Cu K_α radiation. To obtain accurate density values, measurements were performed under low-humidity conditions to avoid an underestimation of the film mesoporosity.

Raman measurements were performed using a "Senterra" Raman microscope (Bruker) under a laser excitation of 638 nm (1 mW power). The spectra were collected with a resolution of ∼3−5 cm^{-1} and an integration time of 10 s.

Femtosecond TA measurements were acquired using a home-built pump−probe setup. The output of a 5 kHz Ti:Sapphire femtosecond amplifier (Spectra-Physics Solstice-Ace) generating 45 fs pulses peaking at 800 nm is split into two beams through a beam-splitter (80/20%) to generate the pump and probe pulses, respectively. The former is obtained by frequency doubling (type I phase-matching) the 800 nm beam to 400 nm through a 250 μm thick beta-BBO crystal and isolated from the fundamental by a Schott BG40 filter. It is then chopped at 2.5 kHz in order to alternatively record the pumped and unpumped spectra. The probe is a supercontinuum pulse covering the 440−750 nm spectral range, obtained by focusing the 800 nm beam on a 1 mm quartz cuvette containing D_2O. A motorized delay stage allows to control the pump−probe relative delay. Both pump and probe are focused and spatially overlapped on the sample under study. After passing through the sample, the transmitted probe is dispersed by a Brewster-angle silica prism and focused by a lens on a single shot detector (Glaz-LineScan I) opportunely triggered. The used configuration guarantees a spectral resolution of 3 nm and a temporal resolution of about 200 fs. All the TA measurements were made in a linear regime, under the so-called magic angle detection conditions. The TA data reported were subjected to standard correction procedures to eliminate the effects of cross-phase modulation and group velocity dispersion.

The photoelectrochemical measurements were realized using a custom-made photoelectrochemical cell, with a standard 3-electrode system [working electrode (WE): nanocomposite film or bare mesoporous titania, reference electrode (RE): Ag/AgCl (KCl 3 M), counter electrode (CE): Pt foil]. Figure 1 shows the setup. A Metrohm Autolab PGSTAT302N potentiostat coupled with Nova software was used. Linear sweep voltammetry was carried out at 50 mV s^{-1} when continuous illumination was used or 10 mV s^{-1} for chopped illumination experiments. The light sources were an Abet Technologies Sun 2000 Solar Simulator, equipped with a 150 Watt Xenon short arc lamp and an irradiating power of 1 sun (air mass, AM 1.5) and a Zolix MLED4-2 UV-LED at 365 nm. Light was shone from the electrode-solution interface. Current densities are referred to the geometrical area of the samples. Potentials were converted to the reversible hydrogen electrode (RHE), according to eq 1:

$$E(\text{vs RHE}) = E(\text{vs Ag/AgCl}) + 0.059 \times \text{pH} \quad (1)$$

The solar light source was set to an intensity of 110 mW cm^{-2}, while the UV led at 100 mW cm^{-2}. The thin films were used as working electrodes, with a Pt wire as the counter electrode and Ag/AgCl (KCl 3 M, E = 0.210 V vs NHE) as reference. The electrolyte used was 0.1 M phosphate buffer solution at pH 7. Current densities refer to the geometrical area.

3. RESULTS AND DISCUSSION

The fabrication of the nanocomposite electrodes relies on the in situ formation and growth of C-dots within a mesoporous ordered titania film (m-TiO_2) (Figure 2). The synthesis is divided into two steps: first, m-TiO_2 films are deposited on different substrates (glass/FTO/silicon wafers) via dip-coating. Afterward, the C-dots are grown in the mesopores by inserting the titania matrix into a reactor for solvothermal synthesis using ethanol as the solvent and phloroglucinol as the C-dot precursor. An alternative route to obtain nanocomposite films using photoactive C-dots is introducing the nanoparticles

https://doi.org/10.1021/acs.chemmater.3c01164
Chem. Mater. 2023, 35, 8009−8019

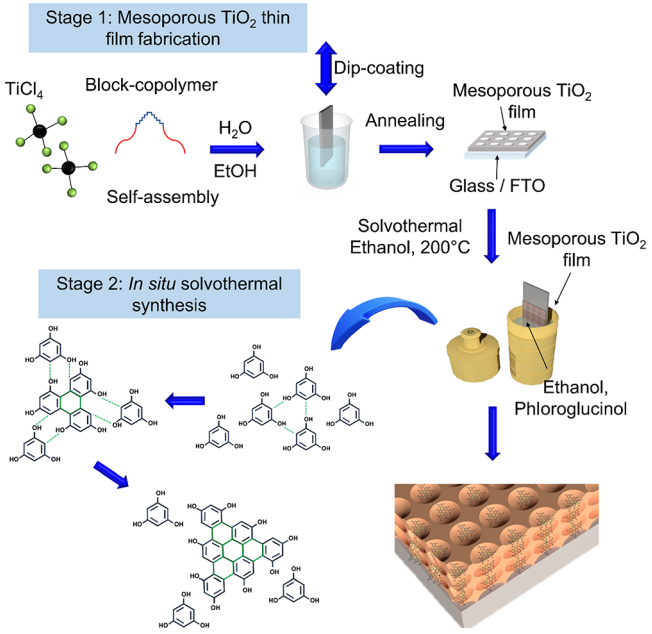

Figure 2. Scheme of the two-stage fabrication of mesoporous titania films containing C-dots. In the first stage, the m-TiO_2 films are deposited on a substrate and afterward annealed at 350 °C. In the second stage, an in situ C-dot solvothermal synthesis to form the nanoparticles within the m-TiO_2 films is employed.

directly into the precursor solution. In this case, however, it is necessary to synthesize in advance C-dots of the same shape and size. Furthermore, the main problem is avoiding aggregation during the deposition of the films. Also, occupying all the pores homogeneously would be very difficult, making the process uncontrollable. Therefore, the in situ synthesis has been designed to overcome these limitations.

After the synthesis, the films show a color change that indicates the successful formation of the C-dots within the titania mesoporous matrix (Figure 3a). The annealed (350 °C)

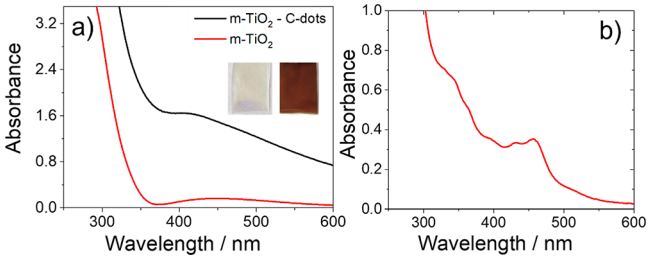

Figure 3. (a) UV−vis absorption spectra of the mesoporous titania films after thermal treatment at 350 °C (red line) and after growing in situ the C-dots (black line). The inset shows the optical appearance of the films before and after C-dots formation. (b) UV−vis absorption spectrum of C-dots in solution as prepared from solvothermal synthesis.

titania films show a broad and weak absorption band peaking at 450 nm generated by the optical interference due to the combination of the thin titania film thickness and its refractive index. The nanocomposite film has an intense absorption band with a maximum of 410 nm that is assigned to n−π^* transitions in C-dots.[37] In turn, the absorption spectrum of C-dots in solution obtained by the solvothermal route shows the presence of different absorption bands in the range of 300−600 nm. The bands are attributed to a vibronic progression of C-dots absorption or the formation of C-dots of different shapes and sizes, in agreement with previous reports for the synthesis of carbon nanostructures using phloroglucinol (Figure 3b).[38] The absorption spectrum of the titania film with C-dots does not show the presence of different bands; the growth of C-dots in a geometrically confined environment, such as that of mesopores, is, in fact, expected to favor the formation of preferentially monodisperse particles.

The band gap (BG) change in the titania matrices after the solvothermal growth of the C-dots has been evaluated by Tauc plots (Figure S1). The BG measured in titania films after heat treatment at 350 °C is 3.9 eV; this value drops to 3.5 eV after solvothermal treatment. The difference is explained by the increase in the degree of crystallinity of the titania matrices when they undergo treatment to form C-dots (vide infra).

Raman spectroscopy analysis of the nanocomposite films reveals both the crystallization of the titania matrix and the presence of polyaromatic carbon structures, according to the formation of C-dots. The Raman spectrum of m-TiO_2 in the 80−800 cm^{-1} shows the presence of four peaks at 145, 398, 515, and 634 cm^{-1}, which correspond to the vibrational modes of $E_g(1)$, $E_g(2)$, $B_{1g}(1)$, A_{1g} + $B_{1g}(2)$, and $E_g(3)$ of anatase TiO_2, respectively (Figure 4a). This result confirms that the designed thermal treatment is enough to induce an early crystallization of the titania matrix into the anatase structure. However, a complete crystallization is generally reached at temperatures higher than 400 °C.[39] Figure 4b shows the spectra of the titania film in the range of 1050−1900 cm^{-1} before and after the solvothermal synthesis. In this range, no Raman signals assigned to titania are detected. After the C-dot formation (red line), the spectrum collected from the sample shows two Raman bands located at about 1318 and 1555 cm^{-1} and associated with D- and G-band of polyaromatic carbon structures.[40] Raman spectra also reveal the presence of a shoulder at 1200 cm^{-1} that is attributed to the −OH bending of the terminal hydroxy-group attached to the benzene rings. FTIR analysis of the nanocomposite film also confirms the presence of the phenol groups. A band peaked at 1300 cm^{-1} and attributed to the $C_{aromatic}$−OH stretching is observed after solvothermal treatment (Figure S2). In carbon-based materials, the G-band of the Raman spectrum is due to in-plane vibrations of sp^2 carbon atoms, whereas the D-band is commonly attributed to nonaromatic sp^3 carbon.[41] The ratio between the peak intensities of the D- and G-bands is, therefore, a parameter to estimate the degree of graphitization of the carbon nanostructures. An I_D/I_G value close to zero is generally obtained from graphene-like 2D structures, such as exfoliated graphene. On the contrary, the largely oxidized graphene oxide gives an I_D/I_G value of 1.2−1.3.[42] Interestingly, the I_D/I_G calculated for the Raman spectrum in Figure 4a is in the range of 1.1. This value is compatible with both not-completely graphitized carbon structures or small graphene fragments, such as CQDs or graphene nanoplatelets, with a size smaller than 50 nm.[41] Considering that the solvothermal synthesis of phloroglucinol at similar temperatures leads to the formation of GQDs,[38] the UV−vis and Raman characterizations well support the hypothesis of the GQD growth within the mesopores.

Figure 5a,b shows representative TEM images of the mesoporous titania matrix before and after the C-dots formation. The images were taken from film fragments scratched from the substrates and ground in a mortar before

https://doi.org/10.1021/acs.chemmater.3c01164
Chem. Mater. 2023, 35, 8009−8019

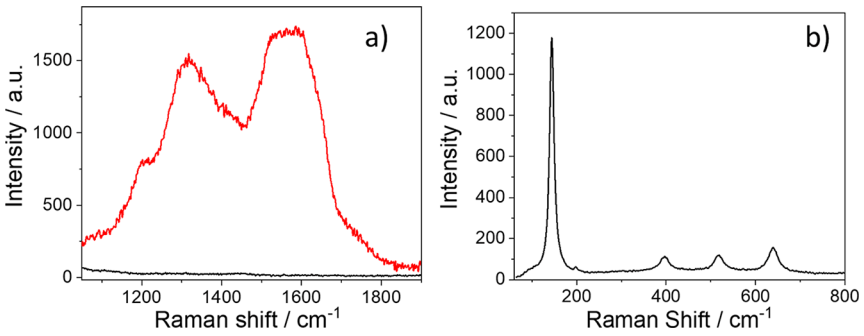

Figure 4. (a) Raman spectra of m-TiO_2 and nanocomposite films in the 1050−1900 cm^{-1} range (black and red lines, respectively). (b) Raman spectrum of m-TiO_2 films deposited on FTO glass in the 80−800 cm^{-1} range.

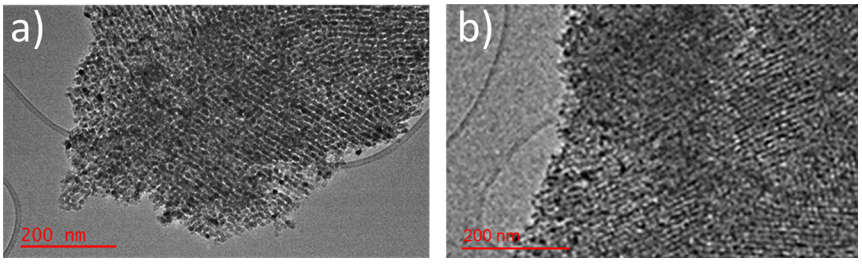

Figure 5. TEM images of mesoporous titania films before (a) and after (b) solvothermal treatment to grow C-dots within the pores.

the analysis. The titania film exhibits a long-range organization of mesopores with a typical $I\bar{3}mm$ symmetry.[43] From the line analysis performed on selected TEM images (see Figure S3), the wall-to-wall distance can be estimated as 10.75 ± 0.7 nm, in accordance with previous results.[13] TEM images taken on mesoporous samples after solvothermal treatment do not show any clear evidence of the presence of carbon nanoparticles. However, a partial loss of electronic contrast in the images can be attributed to the formation of carbon nanostructures in the pores.

X-ray reflectivity (XRR) and spectroscopic ellipsometry have been used to verify the pore filling after the C-dot growth and/or the eventual formation of a carbon layer onto the titania film. Figure S4 shows the X-ray reflectograms of m-TiO_2 before and after solvothermal synthesis. The critical angle, θ_c, increases from 0.48 to 0.50°, due to the C-dot growth in the mesopores, suggesting a reduction in porosity. This reduction is consistent with the presence of C-dots within the mesoporous network and explains the possible changes in the refractive index.

In agreement with the XRR analysis, spectroscopic ellipsometry also shows a substantial reduction of the pore volume once the C-dots nucleate in the mesoporous matrix. Table 1 reports the calculated pore volume (voids) value in an m-TiO_2 sample as obtained using an effective medium approximation model to analyze the experimental data. In addition, the refractive index of the mesoporous titania matrix has been retrieved by measuring a reference sol−gel dense titania film treated at 350 °C. After solvothermal synthesis, the pore volume decreases from 26 to 12%, more than 50% of the initial value, indicating a remarkable filling of the porous structure.

Table 1. Thickness and Pore Volume Measured by Ellipsometry for the Mesoporous Titania Films before and after the Solvothermal Synthesis

	before solvothermal treatment	after solvothermal treatment
thickness, nm	161.4 ± 1.7	182.3 ± 2.0
pore volume, %	26 ± 2	12.0 ± 5

To investigate the microstructure changes in the titania mesoporous matrix induced by C-dots growth, X-ray absorption near-edge structure (XANES) analysis has also been applied. The anatase phase of titanium dioxide has been thoroughly studied by XANES,[44,45] especially in the Ti K pre-edge region, to detect changes in the local Ti coordination associated with different postsynthesis treatments. Figure 6 shows the differences in the pre-edge of Ti K among the film after thermal treatment (green line), the film after solvothermal growth of C-dots (red line), and the film after solvothermal treatment in pure ethanol used as reference (blue line). Following previous attributions,[46] the high energy resolution allows the identification of four pre-edge signals, named A1,

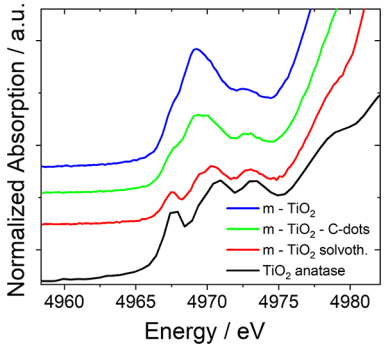

Figure 6. XANES in the pre-edge Ti K range of a mesoporous titania film after thermal treatment at 350 °C (blue line); after solvothermal growth of C-dots (green line); and after solvothermal treatment in pure ethanol (red line). The XANES spectrum of the TiO_2 in the anatase polymorph is reported as the reference (black line).

https://doi.org/10.1021/acs.chemmater.3c01164
Chem. Mater. 2023, 35, 8009−8019

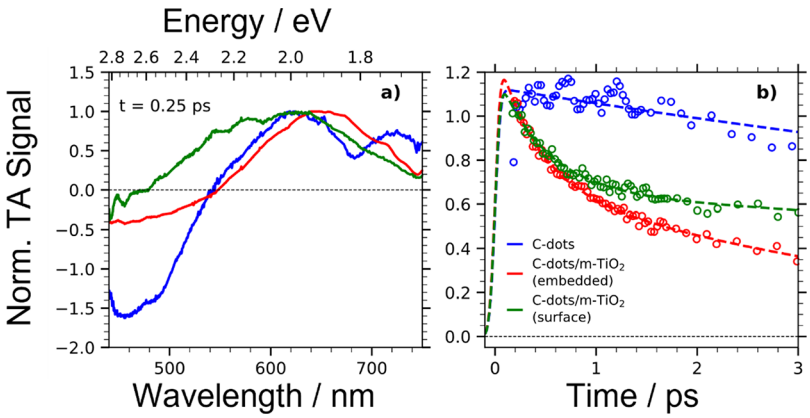

Figure 7. (a) Comparison of normalized TA spectra of an aqueous solution of C-dots (blue), C-dots embedded into m-TiO_2 film (red) and deposited postsynthesis on the surface of an m-TiO_2 film (green) taken at a pump−probe delay of 0.25 ps under a pump excitation of 400 nm. (b) Kinetic traces cut at the probe wavelength of 570 nm and associated fitting curves of an aqueous solution of C-dots (blue), C-dots embedded into m-TiO_2 film (red) and deposited postsynthesis on the surface of an m-TiO_2 film (green).

A2, A3, and B (and peaked at 4967, 4969, 4971, and 4973 eV) in the spectra (Figure S5a−c). The peaks are due to the transitions of the core electron to Ti 3d4p4s hybridized states.

A distortion of the octahedral TiO_6 unit in the film produces stronger contributions from the A2 and A3 components in the pre-edge region. It indicates a lower degree of anatase-like crystallization in the thermally treated m-TiO_2.[45] The fraction of anatase in each sample has been calculated according to previous work (Figure S5d,e).[46] Mesoporous titania samples treated at 350° and then subjected to solvothermal synthesis without using C-dots precursors show a configuration of tetrahedral units more similar to anatase than in films treated only thermally at 350 °C. The thermally treated m-TiO_2 sample has a 16% anatase content, whereas the solvothermal treated shows an anatase fraction of 55%, which decreases to 33% for m-TiO_2−C-dot nanocomposite films.

XANES characterization shows that the solvothermal treatment improves the crystallization through relatively mild postsynthesis processing of a partially crystallized titania. Otherwise, to obtain a crystallinity above 35% on glass substrates, heat treatments above 500 °C or resorting to dense buffer underlayers are required.[46,47] The improved crystallization of titania frameworks after solvothermal treatment (either in the presence or absence of C-dot precursors) is in good agreement with the smaller BGs observed (and calculated) in the m-TiO_2−C-dot with respect to bare m-TiO_2 after treatment at 350 °C (Figure S1).

Interestingly, the local rearrangement of the octahedral TiO_6 units that leads to wall crystallization is reduced when phloroglucinol is added to the solvothermal treatment. Polyphenols such as phloroglucinol can readily adsorb through coordination on the pore surface mesoporous titania.[48] We hypothesize that the phloroglucinol adsorption on the pore surface, followed by a fast condensation and C-dot formation, hampers the dissolution and further reconstruction to anatase of the titania surface. On the other hand, complexation by the phenol groups stabilizes the interactions between the forming C-dots and the titania matrix. This condition is essential to establishing ligand-to-metal optical transitions that could aid electron transfer from C-dots to the TiO_2 conduction band (vide infra).

The nanocomposite films obtained from m-TiO_2 do not show photoluminescence, indicating that the interaction with the matrix quenches the typical radiative process occurring in the C-dots (Figure S6a). On the contrary, when a mesoporous silica film is used instead of titania, an emission typical of the C-dots can be observed from the nanocomposites (Figure S6b) in agreement with previous results.[49] A different interaction of the C-dots with the matrix is also evident considering that the C-dots nucleated within mesoporous silica do not color the films, and they can be easily released by rinsing the sample with ethanol (Figure S7). On the contrary, the C-dots nucleated into the mesoporous titania matrix give a homogeneous brown color to the films (inset of Figure 3a). They do not leach out from the samples even after sonication for more than 15 min in ethanol.

The photophysical features of the C-dots, both in suspension or embedded within the mesoporous titania matrix, have been further investigated by ultrafast TA spectroscopy. Figure 7a shows the normalized TA spectra of the three samples taken at a pump−probe delay of 250 fs. The samples are, respectively, C-dots in water (blue line) used as a reference, C-dots grown within the mesoporous titania matrix (red line), and C-dots deposited after the synsthesis on the surface of the mesoporous titania matrix (green line). The reference spectrum of the aqueous solution of C-dots is characterized by a negative signal peaking at 460 nm attributed to a ground state bleaching (GSB) contribution as it spectrally matches the steady-state absorption (Figure 3b). Two positive bands around 630 and 730 nm are associated with excited state absorption (ESA) transitions. The TA spectrum of C-dots nucleated into the m-TiO_2 matrix, as well as C-dots deposited on m-TiO_2, displays a similar shape, but a less structured ESA contribution with a strong increase of the ESA/GSB ratio. These differences in shape between the TA spectra, found already at 250 fs, point out the existence of ground state C-dots/TiO_2 interactions or/and a photoinduced electron transfer from C-dots to TiO_2 occurring within the 200 fs temporal resolution provided by the TA setup. This finding is perfectly compatible with the already discussed PL quenching of C-dots in the titania-based nanocomposite film (Figure S5b). On these grounds, the PL quenching can be explained as a result of ultra-efficient excited-state charge transfer from the excited state in C-dots to the conduction band of titania occurring within 200 fs from photoexcitation.

https://doi.org/10.1021/acs.chemmater.3c01164
Chem. Mater. 2023, 35, 8009−8019

However, the most significant change in the TA signal of the samples is related to its temporal evolution. Figure 7b displays a comparison of the normalized TA kinetic traces of the three samples at a probe wavelength of 570 nm, in correspondence to the ESA contribution. As can be noted, the TA signals of both the C-dots embedded into (red) as well as the C-dots deposited postsynthesis on (green) the m-TiO_2 film are affected by a sub-ps decay that is not found in the C-dots prepared by solvothermal synthesis without the addition of an m-TiO_2 film (blue). This decay can account for a back-electron transfer process whose faster timescales were found to be 390 ± 30 and 480 ± 50 fs for C-dots embedded into and C-dots deposited postsynthesis on the TiO_2 film, respectively.

Previous results have shown that the solvothermal synthesis developed for the growth of C-dots in mesoporous films enables the construction of a functional platform whose properties are governed by the anatase titania-graphene quantum dots heterostructure. In particular, the nucleation and growth of C-dots into m-TiO_2 films allow the designing of nanocomposite matrices with improved photoelectrochemical performances. To investigate the photoelectrochemical properties of the samples, linear sweep voltammetry (LSV) and chronoamperometry measurements have been performed. The measures taken from the nanocomposites have been compared to those of pure mesoporous ordered titania matrices that did not undergo any posttreatment process besides thermal annealing. All the films have been tested in a photoelectrochemical cell upon exposure to a solar simulator.

Figure 8 shows the current density measured in m-TiO_2 films with an applied potential in the dark and under the

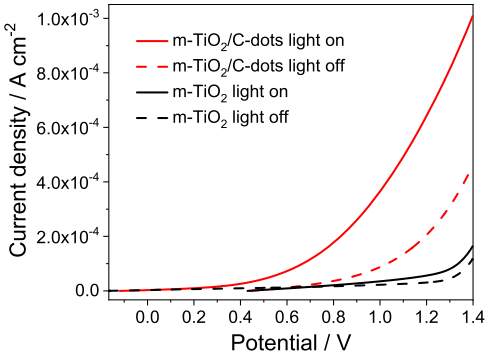

Figure 8. LSV measurements of m-TiO_2 film (black lines) and nanocomposite samples (red lines) upon exposure to radiation with a solar simulator. The full lines show the electrical response with the solar simulator on, whereas the dashed lines with the light source off.

illumination of a solar simulator. In the dark, the current density is zero until an applied voltage of 1.2 V is reached; 1.2 V is the threshold of the electrochemical overpotential needed for water oxidation. As the potential reaches 1.4 V, a current of 10^{-4} A cm^{-2} is measured. This current does not change significantly if the sample is under dark conditions or illuminated, according to the properties of the bare mesoporous titania films.

On the contrary, the nanocomposite samples show a quite different response, both in terms of overpotential and current density. When the sample is illuminated, the current begins to rise at 0.2 V, due to the photogeneration of charge carriers. The holes drive the oxygen formation through OER at the electrode−electrolyte interface, whereas the electrons are driven into the external circuit and reduce water at the Pt counter electrode. In the nanocomposite, the C-dots play a double role. TA measurements demonstrate that, after visible light excitation, the C-dot electrons efficiently transferred to the titania conduction band, in 200 fs time scale (Figure 7), producing holes localized in the HOMO of the C-dots. These holes reduce water by forming oxygen, and, as a consequence of this process, a drop in the overpotential is observed, in this case to 0.2 V. The enhanced current density recorded under illumination results, therefore, from the C-dot sensitization of the titania matrix. In fact, at a potential of 1.4 V, the current rises to 1 mA cm^{-2}.[50]

Figure 9 shows the LSV curves for m-TiO_2 and m-TiO_2−C-dots-nanocomposites under illumination with 365 and 450 nm

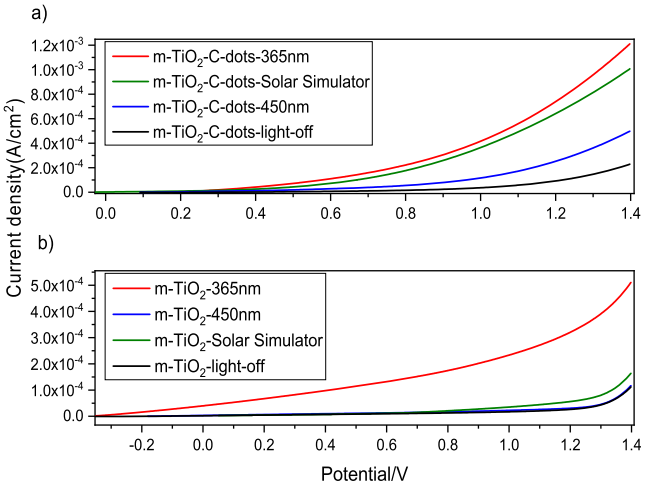

Figure 9. LSV measurements of the m-TiO_2 film (black lines) and nanocomposite samples upon exposure to radiation with a solar simulator (green line), LED 365 nm (red line), and 450 nm (blue line). (a) Measurements of nanocomposite m-TiO_2-Cdots film and (b) m-TiO_2 film.

light-emitting diodes (LEDs) and a solar simulator. The solvothermal growth of C-dots in mesoporous films causes an increase in the photoelectrochemical response in samples illuminated with different light sources. In the UV range, the enhancement is due to two factors. The first is the lower titania BG induced by the solvothermal treatment. The other factor is the presence of the C-dots in the film that also absorb the UV (ca. 3.5 eV, Figure 3) and can increase the light harvesting. Under illumination with the blue LED, the increase in the photocurrent is only due to C-dots because in that wavelength titania does not absorb light. This clearly demonstrates the sensitizing role of the C-dots in the nanocomposite array, which aligns with the charge transfer reported by TA spectroscopy. The response with the solar simulator highlights the synergistic effect of titania anatase with C-dots. To further study this effect, experiments have been also realized with a white lamp (enon) while filtering out the UV radiation. Figure S8 showcases the LSV curves and chronoamperometry results for m-TiO_2 and m-TiO_2−C-dots. By filtering the UV radiation, we observed that the photocurrent generated in the samples with C-dots, both with and without illumination, increases compared to pure titania. In contrast, the current in the pure titania sample does not show considerable changes with or without light. From Figure S8b, it is evident that the increase in photocurrent is 67% compared to m-TiO_2, attributing this

https://doi.org/10.1021/acs.chemmater.3c01164
Chem. Mater. 2023, 35, 8009−8019

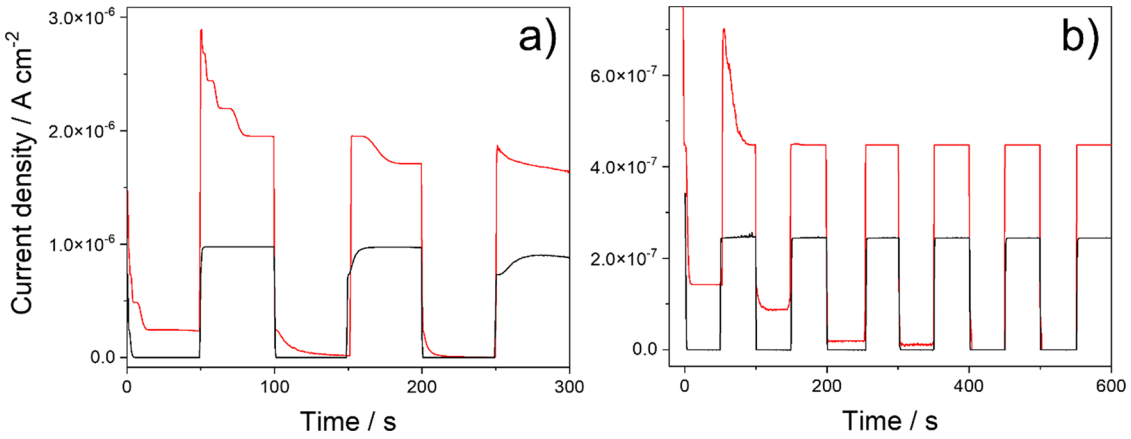

Figure 10. Chronoamperometry of the bare mesoporous titania (black line) and nanocomposite films (black and red lines) at 0.6 V when illuminated with a 365 nm LED (a) and solar simulator (b). The light source was alternatively turned on and off every 50 s.

enhancement to the presence of carbon dots. Further improvements in the nanocomposite performances could be achieved by increasing the degree of crystallinity of the titania matrices and depositing thicker electrodes with higher light-harvesting capability.

According to the LSV measurements, the chronoamperometry measurements at 0.6 V (vs RHE) with chopped illumination, both with UV and visible light, show an increase in the photocurrent when C-dots are nucleated inside the film. Figure 10 shows the comparison between the m-TiO_2 with respect to the nanocomposite electrodes. The current density during the chronoamperometry cycles doubles the intensity after illumination with both UV and visible light reaching 2.0×10^{-6} and 4.5×10^{-6} A cm^{-2}, respectively.

As previously discussed, two factors contribute to the increase in the photocurrent: the crystallinity of the sample and the double role of C-dots. This indicates that the C-dots act partially as sensitizers and contribute to charge carrier transfer and separation in the photoelectrocatalysis of m-TiO_2.

The charge transfer in the TiO_2−C-dots heterostructured system can be qualitatively understood through the energy diagram shown in Figure 11.

The results have been compared with a previous study conducted by Titirici and colleagues, who also examined charge transfer properties for N-doped-C-dots deposited onto TiO_2 nanoparticles.[34] These authors reported that the energy difference between the bands in the nanocomposite was 3.5 eV, indicating the presence of individual energy states that allow energy transitions over a wide range, a similar value for the band gap as obtained in our systems. Based on these findings, a possible charge transfer mechanism can be proposed. Under simulated solar irradiation, electrons in the lower band of C-dots (2.7 eV) and the valence band of TiO_2 (3.6 eV) are efficiently excited and transferred to higher energy levels, either in the conduction band of titania or in the upper band of the C-dots. The resulting holes in the valence band of TiO_2 are transferred to the solution and participate in water oxidation. On the other hand, electrons from the excited C-dots are injected into TiO_2 (as demonstrated by the TA experiments). This electron transfer might hinder recombination, increasing the hole lifetime. The electrons in the CB of titania then can be directed toward the working electrode, and through the external circuit, electrons travel to the counter electrode, where reduction reactions take place. This can be a plausible explanation for the observed effect of increased photocurrents in the case of the C-doped samples.

Figure 12 shows the stability test of the nanocomposite samples, measured at 1.2 V with the solar simulator for 50 min. The illumination has been alternatively kept on and off every 5 min to check the stability in the current density with time. After five cycles and 48 min, the current density decreases by

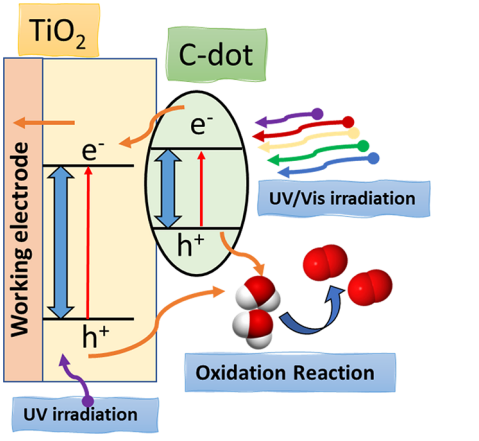

Figure 11. Scheme of the proposed charge separation and transfer pathways between C-dots and m-TiO_2 under solar simulator irradiation.

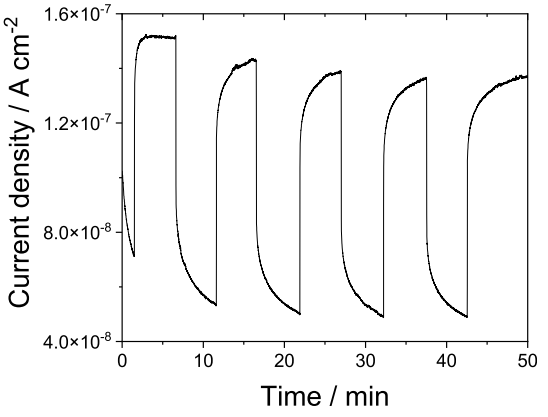

Figure 12. Stability test of the nanocomposite titania electrode after five illumination/dark cycles of 10 min.

https://doi.org/10.1021/acs.chemmater.3c01164
Chem. Mater. 2023, 35, 8009−8019

less than 10%. This result proves the better stability of the m-TiO_2/C-dots photoelectrode compared with other mesoporous ordered titania-based systems, such as porphyrin-sensitized TiO_2 films.[51] In that case, a gradual leakage of the sensitizer is generally observed in the electrodes caused by the electrolyte in solution. This is responsible for a gradual loss of current density that can be estimated at around 50% in a similar time range. In the present case, the strong chemical interaction between the titania and the in situ-grown nanoparticles prevents C-dots from being released from the film, avoiding a loss of photocurrent density.

4. CONCLUSIONS

Ordered mesoporous titania films incorporating C-dots have been obtained by in situ growth of nanoparticles during solvothermal synthesis. The interaction between titania and C-dots allows the preparation of optical-grade nanocomposites that are not fluorescent and favors the electron transfer from the C-dots to the nanocrystalline anatase. The Raman analysis reveals the formation of polyaromatic structures that are not fluorescent when nucleated in the titania matrix but are emissive in silica mesoporous matrices. The emissive properties, the nanometric size, and the polyaromatic structures are all compatible with the formation of graphene quantum dots, as already observed for the solvothermal synthesis of carbon nanoparticles through phloroglucinol. In addition, the C-dots are retained within the titania matrices and do not show nanoparticle leakage after washing. In situ solvothermal synthesis of C-dots represents an optimized method for designing robust photoelectrodes with stable performances over time. This is due to the heterogeneous nucleation within the mesopores that does not allow the C-dots leakage after their synthesis. The complexation ability of the polyphenol precursors on the titania surface can be responsible for the interaction between the forming C-dot and the inorganic matrix. This interaction will also favor ligand-to-metal optical transitions that constitute a channel for enhanced light absorption.

Moreover, LSV experiments on the nanocomposite films allow measuring a very low overpotential, despite the low current density. However, this value could be further optimized by increasing the degree of crystallization of the inorganic matrix and the electrode thickness. The nanocomposite has a notable increase in photocurrent with respect to the bare mesoporous titania film. TA measurements suggest that such an enhancement stems from ultrafast electron transfer (faster than 200 fs) from C-dots excited by visible light to the conduction band of TiO_2. The coupling between the matrix and the C-dots is much more robust than that obtained by postimpregnation processing, and only a 10% reduction in the photocurrent is observed after around 1 h of the test. Using the ordered and monodisperse mesopores as nanoreactors for the solvothermal nucleation and growth of C-dots appears as an alternative, reproducible, and feasible route to design hybrid nanocomposites formed by active matrices interacting with guest nanoparticles. The presence of C-dots in the mesoporous ordered titania matrix leads to a cooperative effect that notably enhances the photoelectrochemical performance.

■ ASSOCIATED CONTENT

Supporting Information

The Supporting Information is available free of charge at https://pubs.acs.org/doi/10.1021/acs.chemmater.3c01164.

Tauc plot obtained from UV−vis spectra of the mesoporous titania films after thermal treatment at 350 °C and after growing in situ the C-dots; FTIR spectra in the 3600−400 cm^{-1} region of the mesoporous TiO_2 and nanocomposite sample; TEM image of a mesoporous titania film treated at 350 °C and relative line profile analysis used to calculate the wall-to-wall distance; X-ray reflectivity curves of the titania mesoporous films, before (black line) and after (red line) the growth of C-dots; X-ray absorption near-edge structure in the pre-edge Ti K range of a mesoporous titania film after thermal treatment, after solvothermal treatment in pure ethanol, and after solvothermal growth of C-dots; 3D excitation−emission−intensity maps of nanocomposite films made of mesoporous ordered silica and titania silica after C-dots solvothermal synthesis; UV−vis spectra and optical appearance of the as-prepared mesoporous silica film, after thermal annealing at 350 °C, after solvothermal synthesis, and after washing with ethanol; and linear sweep voltammetry and chronoamperometry after illumination with a Xenon lamp with a UV filter of m-TiO_2 films and nanocomposite samples (PDF)

■ AUTHOR INFORMATION

Corresponding Authors

Luca Malfatti − *Laboratory of Materials Science and Nanotechnology (LMNT), Department of Biomedical Sciences, University of Sassari, CR-INSTM, Sassari 07100, Italy;* orcid.org/0000-0001-6901-8506; Email: luca.malfatti@uniss.it

Plinio Innocenzi − *Laboratory of Materials Science and Nanotechnology (LMNT), Department of Biomedical Sciences, University of Sassari, CR-INSTM, Sassari 07100, Italy;* orcid.org/0000-0003-2300-4680; Email: plinio@uniss.it

Authors

Facundo C. Herrera − *Instituto de Nanosistemas, Escuela de Bio y Nanotecnologías, Universidad Nacional de San Martín-CONICET, San Martín, Buenos Aires B1650, Argentina*

Veronica Sireus − *Laboratory of Materials Science and Nanotechnology (LMNT), Department of Biomedical Sciences, University of Sassari, CR-INSTM, Sassari 07100, Italy*

Pietro Rassu − *Laboratory of Materials Science and Nanotechnology (LMNT), Department of Biomedical Sciences, University of Sassari, CR-INSTM, Sassari 07100, Italy*

Luigi Stagi − *Laboratory of Materials Science and Nanotechnology (LMNT), Department of Biomedical Sciences, University of Sassari, CR-INSTM, Sassari 07100, Italy;* orcid.org/0000-0002-7238-8425

Marco Reale − *Department of Physics and Chemistry (DiFC) "E. Segrè", University of Palermo, Palermo 90123, Italy*

Alice Sciortino − *Department of Physics and Chemistry (DiFC) "E. Segrè", University of Palermo, Palermo 90123, Italy; ATeN Center—University of Palermo, Palermo 90128, Italy;* orcid.org/0000-0001-8361-3002

Fabrizio Messina − *Department of Physics and Chemistry (DiFC) "E. Segrè", University of Palermo, Palermo 90123, Italy; ATeN Center—University of Palermo, Palermo 90128, Italy;* orcid.org/0000-0002-2130-0120

https://doi.org/10.1021/acs.chemmater.3c01164
Chem. Mater. 2023, 35, 8009−8019

Galo J. A. A. Soler-Illia − *Instituto de Nanosistemas, Escuela de Bio y Nanotecnologías, Universidad Nacional de San Martín-CONICET, San Martín, Buenos Aires B1650, Argentina;* orcid.org/0000-0001-9984-3806

Complete contact information is available at: https://pubs.acs.org/10.1021/acs.chemmater.3c01164

Author Contributions

Conceptualization, L.M., G.J.A.A.S.-I., and P.I.; methodology, V.S., F.H., and P.R.; investigation, V.S., F.H., P.R., L.S., M.R., A. S., and F. M.; writing—original draft preparation, F.H., V.S., P.R., L.S., and M.M.; writing—review and editing, L.M., F.H., G.J.A.A.S.-I., and P.I.; supervision, L.M., L.S., and G.J.A.A.S.-I., project administration, L.M.; funding acquisition, L.M and G.J.A.A.S.-I. All authors have read and agreed to the published version of the manuscript.

Funding

Italian Ministry of Foreign Affairs and International Cooperation (grant PGR07324) is gratefully acknowledged for their financial support. This research was funded by the Ministry of Education, University, and Researcher (MIUR) grant number PRIN 2017 "CANDL^2" n.2017W75RAE. The work has been also developed within the framework of the project e.INS Ecosystem of Innovation for Next Generation Sardinia (cod. ECS 00000038) funded by the Italian Ministry for Research and Education (MUR) under the National Recovery and Resilience Plan (NRRP)-MISSION 4 COMPONENT 2, "From research to business" INVESTMENT 1.5, "Creation and strengthening of Ecosystems of innovation" and construction of "Territorial R&D Leaders". G.J.A.A.S.-I. acknowledges support from Agencia I + D + I (PICT 2018-04236 and PICT 2020-03130). F.C.H. thanks ICTP and ELETTRA-CERIC for providing the funding and the facilities for the synchrotron radiation experiment number 20210254. We thank in particular Luca Olivi, Danilo Oliveira, and Giuliana Aquilanti for the support.

Notes

The authors declare no competing financial interest.

■ ACKNOWLEDGMENTS

M. Pilo, G. Mulas, and M. Poddighe are gratefully acknowledged for experimental support.

■ REFERENCES

(1) Innocenzi, P.; Malfatti, L. Mesoporous Thin Films: Properties and Applications. *Chem. Soc. Rev.* **2013**, *42*, 4198−4216.
(2) Alvarez-Fernandez, A.; Reid, B.; Fornerod, M.; Taylor, A.; Divitini, G.; Guldin, S. Structural Characterization of Mesoporous Thin Film Architectures: A Tutorial Overview. *ACS Appl. Mater. Interfaces* **2020**, *12*, 5195−5208.
(3) Etienne, M.; Quach, A.; Grosso, D.; Nicole, L.; Sanchez, C.; Walcarius, A. Molecular Transport into Mesostructured Silica Thin Films: Electrochemical Monitoring and Comparison between p6m, P63/mmc, and Pm3n Structures. *Chem. Mater.* **2007**, *19*, 844−856.
(4) Innocenzi, P. Mesoporous ordered films via self-assembly: trends and perspectives. *Chem. Sci.* **2022**, *13*, 13264−13279.
(5) Innocenzi, P.; Malfatti, L.; Kidchob, T.; Falcaro, P. Order-Disorder in Self-Assembled Mesostructured Silica Films: A Concepts Review. *Chem. Mater.* **2009**, *21*, 2555−2564.
(6) Innocenzi, P.; Malfatti, L. Nanoparticles in mesoporous films, a happy marriage for materials science. *J. Nanopart. Res.* **2018**, *20*, 167.
(7) Angelomé, P.; Pastoriza-Santos, I.; Pérez-Juste, J.; Rodríguez-González, B.; Zelcer, A.; Soler-Illia, G. J. A. A.; Liz-Marzán, L. M. Growth and branching of gold nanoparticles through mesoporous silica thin films. *Nanoscale* **2012**, *4*, 931−939.
(8) Malfatti, L.; Falcaro, P.; Marmiroli, B.; Amenitsch, H.; Piccinini, M.; Falqui, A.; Innocenzi, P. Nanocomposite mesoporous ordered films for lab-on-chip intrinsic surface enhanced Raman scattering detection. *Nanoscale* **2011**, *3*, 3760−3766.
(9) Martínez, E. D.; Boissière, C.; Grosso, D.; Sanchez, C.; Troiani, H.; Soler-Illia, G. J. A. A. Confinement-Induced Growth of Au Nanoparticles Entrapped in Mesoporous TiO_2 Thin Films Evidenced by in Situ Thermo-Ellipsometry. *J. Phys. Chem. C* **2014**, *118*, 13137−13151.
(10) Buso, D.; Falcaro, P.; Costacurta, S.; Guglielmi, M.; Martucci, A.; Innocenzi, P.; Malfatti, L.; Bello, V.; Mattei, G.; Sada, C.; Amenitsch, H.; Gerdova, I.; Haché, A. PbS-Doped Mesostructured Silica Films with High Optical Nonlinearity. *Chem. Mater.* **2005**, *17*, 4965−4970.
(11) Marongiu, D.; Carboni, D.; Malfatti, L.; Innocenzi, P. Pore-confined synthesis of mesoporous nanocrystalline La−Ce phosphate films for sensing applications. *J. Mater. Chem.* **2012**, *22*, 20498−20503.
(12) Malfatti, L.; Carboni, D.; Pinna, A.; Lasio, B.; Marmiroli, B.; Innocenzi, P. In situ growth of Ag nanoparticles in graphene/TiO_2 mesoporous films induced by Hard X-ray. *J. Sol-Gel Sci. Technol.* **2016**, *79*, 295−302.
(13) Pinna, A.; Lasio, B.; Piccinini, M.; Marmiroli, B.; Amenitsch, H.; Falcaro, P.; Tokudome, Y.; Malfatti, L.; Innocenzi, P. Combining Top-Down and Bottom-Up Routes for Fabrication of Mesoporous Titania Films Containing Ceria Nanoparticles for Free Radical Scavenging. *ACS Appl. Mater. Interfaces* **2013**, *5*, 3168−3175.
(14) Costacurta, S.; Malfatti, L.; Innocenzi, P.; Amenitsch, H.; Masili, A.; Corrias, A.; Casula, M. F. Confined growth of iron cobalt nanocrystals in mesoporous silica thin films: FeCo-SiO_2 nanocomposites. *Microporous Mesoporous Mater.* **2008**, *115*, 338−344.
(15) Martínez, E. D.; Bellino, M. G.; Soler-Illia, G. J. A. A. Patterned Production of Silver−Mesoporous Titania Nanocomposite Thin Films Using Lithography-Assisted Metal Reduction. *ACS Appl. Mater. Interfaces* **2009**, *1*, 746−749.
(16) Innocenzi, P.; Malfatti, L.; Carboni, D. Graphene and carbon nanodots in mesoporous materials: an interactive platform for functional applications. *Nanoscale* **2015**, *7*, 12759−12772.
(17) Suzuki, K.; Malfatti, L.; Carboni, D.; Loche, D.; Casula, M.; Moretto, A.; Maggini, M.; Takahashi, M.; Innocenzi, P. Energy Transfer Induced by Carbon Quantum Dots in Porous Zinc Oxide Nanocomposite Films. *J. Phys. Chem. C* **2015**, *119*, 2837−2843.
(18) Ding, H.; Zhou, X.-X.; Zhang, Z.-H.; Zhao, Y.-P.; Wei, J.-S.; Xiong, H.-M. Large scale synthesis of full-color emissive carbon dots from a single carbon source by a solvent-free method. *Nano Res.* **2022**, *15*, 3548−3555.
(19) Hola, K.; Zhang, Y.; Wang, Y.; Giannelis, E. P.; Zboril, R.; Rogach, A. L. Carbon dots—Emerging light emitters for bioimaging, cancer therapy and optoelectronics. *NANO* **2014**, *9*, 590−603.
(20) Zhang, L.; Yang, X.; Yin, Z.; Sun, L. A review on carbon quantum dots: synthesis, photoluminescence mechanisms and applications. *Luminescence* **2022**, *37*, 1612−1638.
(21) Fu, M.; Ehrat, F.; Wang, Y.; Milowska, K. Z.; Reckmeier, C.; Rogach, A.; Stolarczyk, J. K.; Urban, A. S.; Feldmann, J. Carbon Dots: A Unique Fluorescent Cocktail of Polycyclic Aromatic Hydrocarbons. *Nano Lett.* **2015**, *15*, 6030−6035.
(22) Zhang, Q.; Wang, R.; Feng, B.; Zhong, X.; Ostrikov, K. Photoluminescence mechanism of carbon dots: triggering high-color-purity red fluorescence emission through edge amino protonation. *Nat. Commun.* **2021**, *12*, 6856.
(23) Ren, J.; Malfatti, L.; Innocenzi, P. Citric Acid Derived Carbon Dots, the Challenge of Understanding the Synthesis-Structure Relationship. *C* **2021**, *7*, 2.
(24) Zhu, S.; Song, Y.; Zhao, X.; Shao, J.; Zhang, J.; Yang, B. The photoluminescence mechanism in carbon dots (graphene quantum dots, carbon nanodots, and polymer dots): current state and future perspective. *Nano Res.* **2015**, *8*, 355−381.

(25) Abbas, A.; Tabish, T.; Bull, S. J.; Lim, T. M.; Phan, A. N. High yield synthesis of graphene quantum dots from biomass waste as a highly selective probe for Fe^{3+} sensing. *Sci. Rep.* **2020**, *10*, 21262.
(26) Đorđević, L.; Arcudi, F.; Cacioppo, M.; Prato, M. A multifunctional chemical toolbox to engineer carbon dots for biomedical and energy applications. *Nat. Nanotechnol.* **2022**, *17*, 112−130.
(27) Tao, S.; Feng, T.; Zheng, C.; Zhu, S.; Yang, B. Carbonized Polymer Dots: A Brand New Perspective to Recognize Luminescent Carbon-Based Nanomaterials. *J. Phys. Chem. Lett.* **2019**, *10*, 5182−5188.
(28) Liu, Y.; Wang, P.; Fernando, K. A. S.; LeCroy, G. E.; Maimaiti, H.; Harruff-Miller, B. A.; Lewis, W. K.; Bunker, C. E.; Houa, Z.-L.; Sun, Y.-P. Enhanced fluorescence properties of carbon dots in polymer film. *J. Mater. Chem. C* **2016**, *4*, 6967−6974.
(29) Kamura, Y.; Imura, K. Space-Selective Fabrication of Light-Emitting Carbon Dots in Polymer Films Using Electron-Beam-Induced Chemical Reactions. *ACS Omega* **2019**, *4*, 3380−3384.
(30) Shauloff, N.; Bhattacharya, S.; Jelinek, R. Elastic carbon dot/polymer films for fluorescent tensile sensing and mechano-optical tuning. *Carbon* **2019**, *152*, 363−371.
(31) Hunter, B. M.; Gray, H. B.; Muller, A. M. Earth-Abundant Heterogeneous Water Oxidation Catalysts. *Chem. Rev.* **2016**, *116*, 14120−14136.
(32) Li, W.; Elzatahry, A.; Aldhayan, D.; Zhao, D. Core−shell structured titanium dioxide nanomaterials for solar energy utilization. *Chem. Soc. Rev.* **2018**, *47*, 8203−8237.
(33) Xie, S.; Hua, S.; Wei, W.; Li, M.; Tong, Y.; Mao, Z. Remarkable photoelectrochemical performance of carbon dots sensitized TiO_2 under visible light irradiation. *J. Mater. Chem. A* **2014**, *2*, 16365−16368.
(34) Luo, H.; Dimitrov, S.; Daboczi, M.; Kim, J.-S.; Guo, Q.; Fang, Y.; Stoeckel, M.-A.; Samorì, P.; Fenwick, O.; Jorge Sobrido, A. B.; Wang, X.; Titirici, M. M. Nitrogen-Doped Carbon Dots/TiO_2 Nanoparticle Composites for Photoelectrochemical Water Oxidation. *ACS Appl. Nano Mater.* **2020**, *3*, 3371−3381.
(35) Carboni, D.; Marongiu, D.; Rassu, P.; Pinna, A.; Amenitsch, H.; Casula, M.; Marcelli, A.; Cibin, G.; Falcaro, P.; Malfatti, L.; Innocenzi, P. Enhanced Photocatalytic Activity in Low-Temperature Processed Titania Mesoporous Films. *J. Phys. Chem. C* **2014**, *118*, 12000−12009.
(36) Malfatti, L.; Falcaro, P.; Pinna, A.; Lasio, B.; Casula, M. F.; Loche, D.; Falqui, A.; Marmiroli, B.; Amenitsch, H.; Sanna, R.; Mariani, A.; Innocenzi, P. Exfoliated Graphene into Highly Ordered Mesoporous Titania Films: Highly Performing Nanocomposites from Integrated Processing. *ACS Appl. Mater. Interfaces* **2014**, *6*, 795−802.
(37) Mura, S.; Ludmerczki, R.; Stagi, L.; Garroni, S.; Carbonaro, C. M.; Ricci, P. C.; Casula, M. F.; Malfatti, L.; Innocenzi, P. Integrating sol-gel and carbon dots chemistry for the fabrication of fluorescent hybrid organic-inorganic films. *Sci. Rep.* **2020**, *10*, 4770.
(38) Yuan, F.; Yuan, T.; Sui, L.; Wang, Z.; Xi, Z.; Li, Y.; Li, X.; Fan, L.; Tan, Z.; Chen, A.; Jin, M.; Yang, S. Engineering triangular carbon quantum dots with unprecedented narrow bandwidth emission for multicolored LEDs. *Nat. Commun.* **2018**, *9*, 2249.
(39) Innocenzi, P.; Malfatti, L.; Kidchob, T.; Enzo, S.; Della Ventura, G.; Schade, U.; Marcelli, A. Correlative Analysis of the Crystallization of Sol−Gel Dense and Mesoporous Anatase Titania Films. *J. Phys. Chem. C* **2010**, *114*, 22385−22391.
(40) Gohda, S.; Saito, M.; Yamada, Y.; Kanazawa, S.; Ono, H.; Sato, S. Carbonization of phloroglucinol promoted by heteropoly acids. *J. Mater. Sci.* **2021**, *56*, 2944−2960.
(41) Puech, P.; Kandara, M.; Paredes, G.; Moulin, L.; Weiss-Hortala, E.; Kundu, A.; Ratel-Ramond, N.; Plewa, J.-M.; Pellenq, R.; Monthioux, M. Analyzing the Raman Spectra of Graphenic Carbon Materials from Kerogens to Nanotubes: What Type of Information Can Be Extracted from Defect Bands? *C* **2019**, *5*, 69.
(42) Thakkar, S.; De Luca, L.; Gaspa, S.; Mariani, A.; Garroni, S.; Iacomini, A.; Stagi, L.; Innocenzi, P.; Malfatti, L. Comparative Evaluation of Graphene Nanostructures in GERS Platforms for Pesticide Detection. *ACS Omega* **2022**, *7*, 5670−5678.
(43) Soler-Illia, G. J. A. A.; Angelomé, P. C.; Fuertes, M. C.; Grosso, D.; Boissière, C. Critical aspects in the production of periodically ordered mesoporous titania thin films. *Nanoscale* **2012**, *4*, 2549−2566.
(44) Notestein, J. M.; Andrini, L. R.; Kalchenko, V. I.; Requejo, F. G.; Katz, A.; Iglesia, E. Structural Assessment and Catalytic Consequences of the Oxygen Coordination Environment in Grafted Ti−Calixarenes. *J. Am. Chem. Soc.* **2007**, *129*, 1122−1131.
(45) Farges, F.; Brown, G. E.; Rehr, J. J. Ti K-edge XANES studies of Ti coordination and disorder in oxide compounds: Comparison between theory and experiment. *Phys. Rev. B* **1997**, *1997*, 56.
(46) Angelomé, P. C.; Andrini, L.; Calvo, M. E.; Requejo, F. G.; Bilmes, S. A.; Soler-Illia, G. J. J. A. Mesoporous Anatase TiO_2 Films: Use of Ti K XANES for the Quantification of the Nanocrystalline Character and Substrate Effects in the Photocatalysis Behavior. *J. Phys. Chem. C* **2007**, *111*, 10886−10893.
(47) Violi, I. L.; Perez, M. D.; Fuertes, M. C.; Soler-Illia, G. J. A. A. Highly Ordered, Accessible and Nanocrystalline Mesoporous TiO_2 Thin Films on Transparent Conductive Substrates. *ACS Appl. Mater. Interfaces* **2012**, *4*, 4320−4330.
(48) Angelome, P. C.; Soler-Illia, G. J. A. A. Organically Modified Transition-Metal Oxide Mesoporous Thin Films and Xerogels. *Chem. Mater.* **2005**, *17*, 322−331.
(49) Chang, Q.; Yang, S.; Xue, C.; Li, N.; Wang, Y.; Li, Y.; Wang, H.; Yangab, J.; Hu, S. Nitrogen-doped carbon dots encapsulated in the mesoporous channels of SBA-15 with solid-state fluorescence and excellent stability. *Nanoscale* **2019**, *11*, 7247−7255.
(50) Liu, J.; Zhao, S.; Li, C.; Yang, M.; Yang, Y.; Liu, Y.; Lifshitz, Y.; Lee, S.-T.; Kang, Z. Carbon Nanodot Surface Modifications Initiate Highly Efficient, Stable Catalysts for Both Oxygen Evolution and Reduction Reactions. *Adv. Energy Mater.* **2016**, *6*, No. 1502039.
(51) Caraballo, R. M.; Vensaus, P.; Herrera, F. C.; Soler Illia, G. J. J. A.; Hamer, M. Zinc porphyrin/mesoporous titania thin film electrodes: a hybrid material nanoarchitecture for photocatalytic reduction. *RSC Adv.* **2021**, *11*, 31124−31130.

https://doi.org/10.1021/acs.chemmater.3c01164
Chem. Mater. 2023, 35, 8009−8019